Experiments in Fluids (2006) 41: 21–33
DOI 10.1007/s00348-006-0141-x

RESEARCH ARTICLE

M. Falchi · G. Provenzano · D. Pietrogiacomi
G. P. Romano

Experimental and numerical investigation of flow control on bluff bodies by passive ventilation

Received: 25 July 2005 / Revised: 16 March 2006 / Accepted: 19 March 2006 / Published online: 14 April 2006

Abstract In this work, the so-called natural or passive ventilation drag reduction method is investigated experimentally and numerically. Passive ventilation is performed by directly connecting the high pressure region at the front of a body to the lower pressure in the near wake using a venting duct; in this manner, a net mass flux is established within the wake. In particular, in aerodynamic applications it appears suitable to attain a global reduction in the drag of a body moving in a fluid and a reduction in turbulence levels by means of a global modification of the body wake. Velocity field investigations using particle image velocimetry measurements and a Reynolds averaged numerical code are employed at moderately high Reynolds numbers to clarify the effectiveness of drag reduction on a vented bluff body. The numerical and experimental results agree qualitatively, but the amount of reduction for the vented body (about 10%) is underestimated numerically. The effectiveness of drag reduction has been proved both for smooth and rough (single strip) models. Direct balance measurements are used for comparisons.

1 Introduction

Drag reduction, particularly in automotive and aeronautic applications, is one of the most investigated topics for its possible benefits in reduction in fuel consumption and improvement in performance. In the subsonic range, the total drag force exerted on a body is due to the sum of the skin friction drag and the pressure or form drag. As the body shape changes, the relevance of each of these two drags also changes; for streamlined bodies, the skin friction drag is the main part (85–90%), while for bluff bodies the form drag is the most important (80–85%). In particular, a bluff body, immersed in a fluid flow, is characterized by a large separated region in the rear part of the body i.e. the wake. The wake is generated by the boundary layer detachment which avoids the pressure recovery; the net result, considering the high values of the pressure in front of the body, is an increase in the form drag.

Natural ventilation is a flow control technique which modifies the bluff body wake and reduces the total drag by acting on the form drag. In this technique, a venting duct connects the high pressure region in front of the body to the low pressure region in the near wake. In this way, the pressure gradient sets up a flow inside the duct with energy levels as high as the free stream, which energises the wake. The destructive interaction of the counter-rotating vortices from the venting duct and the external shear layer, generating a sort of aerodynamic streamlining, partially destroys the wake and raises the pressure values (behind the body) allowing pressure recovery. The main effect is a large reduction in the form drag together with the reduction in the turbulence intensity in the wake region (Roshko 1961; Aschenbach 1972, 1974; Suryanarayana and Meier 1985; Gad el Hak 2000). It is important to note that no external power is required to generate the improvement in comparison with most other drag reduction (active) techniques, e.g. base bleed, suction or near wake-heating (Monkewitz 1992). Up to now, its effectiveness has been proved only in the case of the sphere (Suryanarayana and Meier 1985; Suryanarayana et al. 1993; Suryanarayana and Prabhu 2000). The results obtained indicate a 50–60% total drag reduction in the supercritical range (i.e. for Reynolds numbers larger than 3.5×10^5 with a fully turbulent boundary layer), while practically no reduction occurs for lower Reynolds numbers. The authors of the previously mentioned papers claim that this is due to the boundary layer transition which helps in transferring momentum from the side of the body and from the outlet of the venting duct to the rest of the wake.

M. Falchi · G. Provenzano · D. Pietrogiacomi
G. P. Romano (✉)
Department of Mechanics and Aeronautics, University of Rome, "La Sapienza", via Eudossiana n. 18, 00184 Rome, Italy
E-mail: romano@dma.ing.uniroma1.it

The main open question concerns the possibility of successfully applying the technique on bluff bodies other than the sphere, which are particularly interesting for industrial applications (it should be considered that many investigations on this aspect are not fully available to the scientific community due to their commercial use). Under this aspect, the typical Reynolds numbers for some applications on vehicles could be lower than the critical Reynolds numbers (for example, for motorcycles or bicycles) so that the performances of natural ventilation should be exploited in subcritical regimes also. To this aim, to attain results similar to those in supercritical regimes, the use of tripping devices in subcritical regimes should be considered.

It must also be noticed that in the sphere the constant curvature allows the boundary layer detachment point to move freely over the sphere surface following changes in the fluid dynamic field (in particular the energy of the shear layers in relation to the wake). This is not allowed in bluff bodies which are more or less truncated in the rear part; that is why it is important to verify the effectiveness of the technique in this case. In particular, based on results of preliminary measurements, the use of a round shape rather than sharp edged bodies in the rear part was considered; this allows comparison of the phenomena observed on the sphere.

In this paper, experiments by particle image velocimetry (PIV) and numerical results by a commercial Reynolds averaged code (RANS) are coupled to investigate the velocity fields around vented and non-vented bluff body models to clarify the above mentioned phenomena, with particular regard to subcritical regimes using round edged tripped bluff bodies. An overall measurement of the drag of different models has been performed by acquiring direct dynamometric balance data.

2 Experimental set-up and numerical simulations

The experimental investigations have been performed in the low speed wind tunnel of the University of Rome "La Sapienza", Italy. The tunnel has an open round test chamber (0.9 m diameter, 1,2 m length), a maximum velocity of 55 m/s, $Re = 2.34 \times 10^6$, and a level of turbulence intensity $< 1\%$. The bluff bodies used to study the effectiveness of the technique are given in Fig. 1a, basic model without venting duct, and Fig. 1b, model with cylindrical venting (different shapes of the duct have been preliminarily considered, the cylindrical one resulting the most effective). This kind of bluff body, a half-sphere on a cylinder with a round corner in the aft region, has been chosen both to maintain some of the aerodynamic features of the sphere and also to investigate a body more similar to automotive applications. The diameter of the model is $D = 14$ cm. An evaluation of the blockage effect is obtained by the ratio of the body to wind tunnel cross-sections, which is about 2.5% i.e. below the threshold of 5% which is indicated as critical for blockage (Rae and Pope 1984). The area of the venting duct cross section is equal to 2.25% of the area of the body cross section, so it is fully feasible in practical applications of the method. Preliminary investigations clarified that round edged models (on the rear side) are more effective for drag reduction in comparison with the sharp edged case (Fig. 1); this is due to the increased possibility of moving the separation point, i.e. to induce larger modifications of the wake. Direct force measurements have been performed using a three component dynamometric balance in order to evaluate the drag component force for a Reynolds number ranging from 2.0×10^5 to 7×10^5.

The model is suspended in the wind tunnel by means of a cylindrical strut (diameter 1.0 cm); the strut is mounted on the opposite side with respect to the measurement region in order to minimise its effect. Thus, velocity data using HWA and PIV are obtained only over one half of the wake (Fig. 2a). For balance measurements, the effect of strut intrusivity has been subtracted to obtain the forces on the body alone; this has been done by combining measurements with the strut alone, with strut connected to the model and with a second strut (non-connected to the model) placed on the other side of the first one (Rae and Pope 1984).

Streamwise velocity component measurements have been performed using hot wire anemometry (HWA) and a Pitot tube with pressure gauge at different positions in the body wakes. For HWA, the sample frequency was equal to 1 kHz; 20,000 samples were acquired at each point. These measurements have been performed at $Re = 3.38 \times 10^5$.

Using a PIV system, equipped by LaVision, (x, y) two component velocity measurements have been performed; the acquired region corresponds to about 2.1 D along the horizontal and 1.6 D along the vertical. The acquisition system is composed by a double Nd-Yag laser, 532 nm wavelength, with 100 mJ per pulse, 7 ns pulse duration. The camera is a cross-correlation one with a $1{,}376 \times 1{,}040$ pixels resolution; the repetition rate of the system is 5 Hz. The seeding particles were olive oil particles with mean diameter of 1 μm.?Each acquisition is made of 1,000 images couples with an optimised time delay between the two images equal to 85 μs. The instantaneous vector field is derived from advanced image deformation recursive PIV cross-correlation algorithms with window offset; the window size is 64×64 pixels with 75% overlapping; thus the spacing between velocity vectors is 16 pixels corresponding to about 3 mm (i.e. 2.5% of the model diameter). This spacing must be considered as the characteristic length to evaluate the spatial resolution of the present PIV velocity measurements. Averaged vector fields have been computed over the 1,000 instantaneous fields as long as other turbulent quantities i.e. turbulence intensities, turbulent kinetic energy and Reynolds stresses. The PIV measurements have been performed at $Re = 1.7 \times 10^5$.

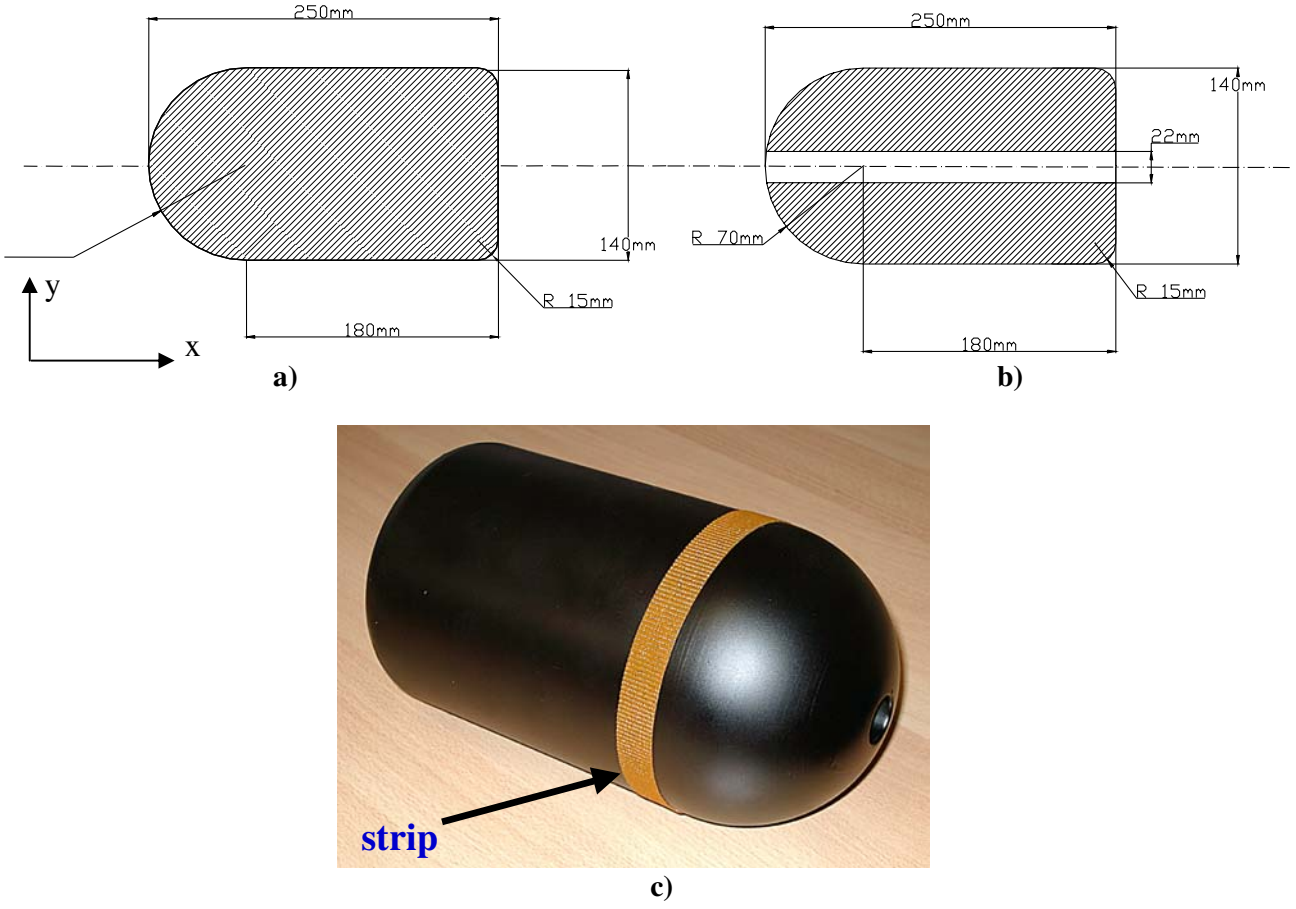

Fig. 1 Bluff body models tested: **a** non-vented or closed model, **b** vented model. The *black painted vented bluff body* in strip configuration (**c**)

It is important to notice that all measurements on the models have been taken both in the smooth or "clean" (no-strip) configuration and in a tripped rough configuration (with "strip"); for the "strip" configuration, an adhesive strip is stuck to the model at the end of the spherical part, while the "clean" configuration is without the strip. This choice allows the boundary layer on the model surface to exploit the transition from laminar to turbulent; thus, the comparison between clean and strip models points out the importance of the boundary layer transition. Moreover, rough models allow us to test the technique in more realistic conditions for practical applications. The strip consists of 1.5 cm wide adhesive paper; in Fig. 1 a picture of the vented model in strip configuration is given (the model is painted in black to reduce reflections in PIV measurements).

The numerical simulations have been performed to test the robustness and suitability for advanced applications of the commercial RANS code used (StarCD) by comparing the data with the experimental ones. The simulations have been performed at a Reynolds number equal to 2.38×10^5, on a fully three-dimensional domain; a high Reynolds number finite volume K-ε model was used with about 3×10^6 cells. The wall function approach with monotone advection and reconstruction scheme (MARS) for average fields and upwind differences for turbulence evaluation have been used. Inlet and outlet profiles have been given at boundaries. Preliminary grid sensitive tests have been performed and a final mesh extending 10 D along all directions has been selected; the residual was 10^{-5} for all variables.

Preliminary flow visualisations using a high speed camera (250 frame/s with resolution equal to 480×420) and a 12W infrared laser, seeding the wind tunnel with smoke have been performed. The Reynolds number for these visualisations is equal to about 5×10^5; this value is within the interval used for direct balance drag measurements and quite close to those used for the other measurement techniques. A couple of acquired images are given in Fig. 2b and c. Although results from instantaneous images must be treated with care (the interval between frames is equal to only 0.4 D/U), the vented case clearly shows a different wake; in particular, the transverse amplitude of the wake seems to be reduced with respect to non-vented conditions. From these visualisations, it is also observed how the venting jet extends up to about one body diameter (this is not always the case for the other tested venting duct, i.e. with smaller diameter or with variable duct geometry) and a clear interaction between the jet itself and the two shear

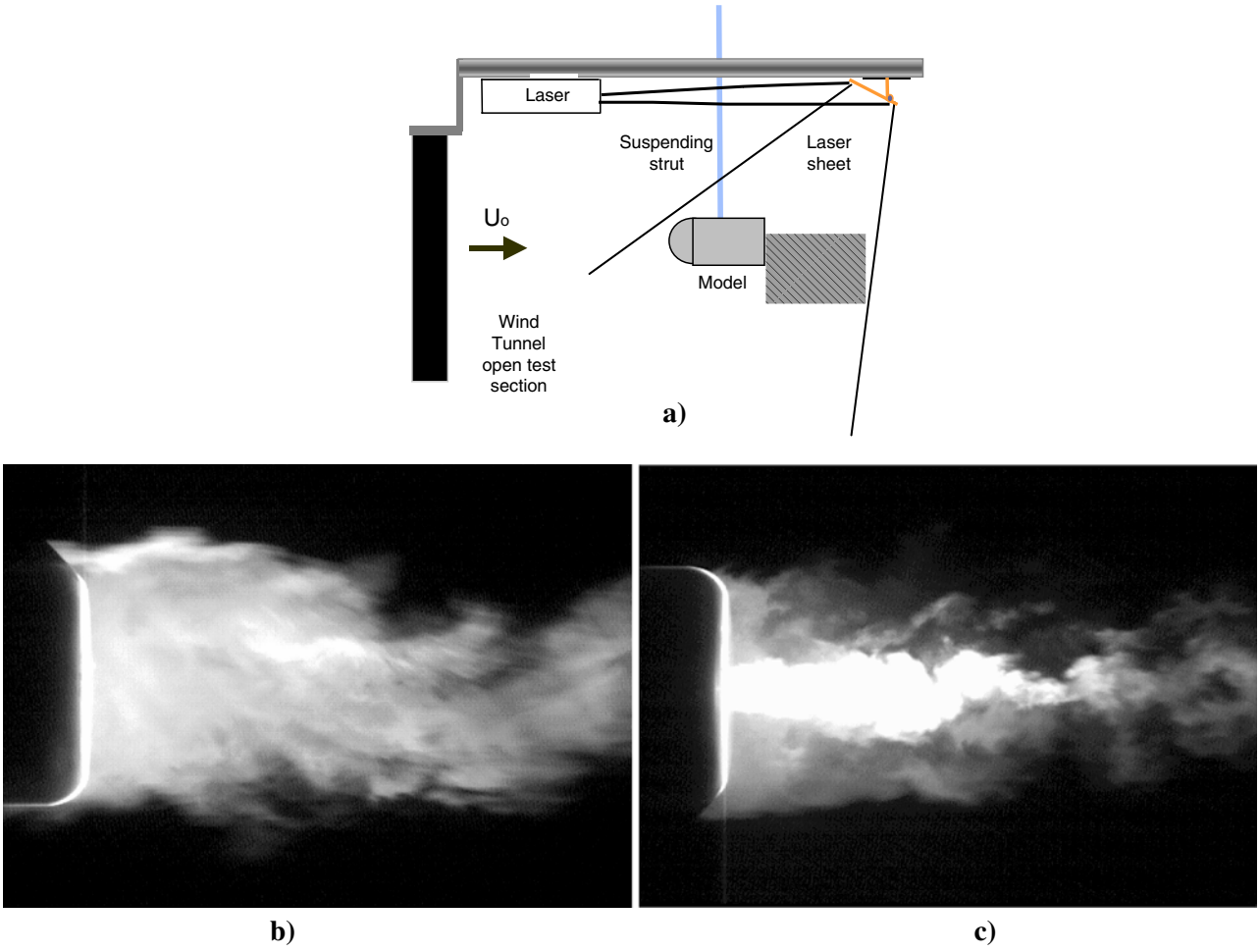

Fig. 2 Experimental set-up: the *dashed area* corresponds to the measurement region (**a**). Smoke visualisation of the **b** non-vented and **c** vented models in strip configuration

layers developing from the body rear side. This interaction reduces the size of the vortical structures in the shear layers in comparison with the non-vented case.

3 Results

3.1 Direct drag measurements

In Fig. 3, the drag coefficient measured with the dynamometric balance as a function of the Reynolds number is depicted for the tested bluff body models; the drag coefficient has been calculated, once the drag, Dr, has been measured, by $C_D = 2Dr/\rho U_\infty^2 S$, where ρ is the air density, U_∞ is the free stream velocity and S is the model cross-sectional area.

As shown in the figure, when comparing non-vented to vented conditions for the clean (no-strip) configuration models, an average drag reduction of about 7–8% is attained; this is slightly larger than the measurement uncertainty (about 5%) and so it must be confirmed by velocity field measurements.

For the strip configurations, a different situation arises; a 20% average drag reduction from non-vented to vented conditions has been obtained. This difference between the no-strip and strip conditions depends on the fact that vented models (in both clean and strip configurations) have almost the same drag, whereas non-vented ones have different values. The non-vented strip model has about 10% higher drag (in comparison with the non-vented clean model) due to forced transition to the fully developed turbulent boundary layer which increases the skin friction drag. Thus, by considering that in practical applications there is always some roughness on the aerodynamic surfaces (which forces boundary layer transition), the technique seems to work much better just in such a situation. In any case, the effect of the venting jet overcomes the boundary layer perturbation due to the strip.

For a deeper understanding of the observed drag reduction, velocity measurements in front and in the wake of the models will be considered. In particular, velocity measurements in the wake allow us to detail the differences occurring in separation regions; on the other

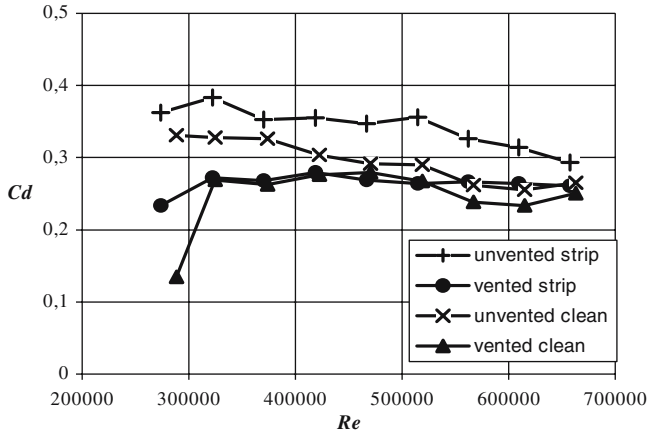

Fig. 3 Direct drag coefficient balance measurements at different Reynolds numbers

hand, the velocity field in front of models is required to compare results with a rather crude evaluation of the drag ratio among vented to non-vented models (by considering the gain in momentum which is obtained in the venting jet). This evaluation gives as a result the ratio of cross-sectional front areas (about 98%); thus, the amount of theoretical drag reduction is only 2%. This value is lower than that observed in the present balance measurements both for clean and strip configurations.

3.2 Velocity measurements

In Fig. 4, instantaneous vector fields (with overlapping axial velocity contours) measured by PIV in the wake of the models are shown for the non-vented and vented conditions (with strip, similar diagrams are obtained for the no-strip case); the upper one half of the model is considered (the black patterns on the left give indication of the model and duct position and size). The reference system origin is located on the rear flat surface, on the cylinder axis; the free stream velocity is directed from left to right. The overall (qualitative) impression from these plots is that the two wakes are very similar; close inspection, however, reveals large vortical structures developing in the shear layer for the non-vented case. These structures, indicated by orange circles in Fig. 4a, contribute towards generating a wide wake even at $x/D = 1.5$. On the other hand, for the vented condition, the interaction between vortical structures from the venting duct and from the shear layer reduces the size of the vortices and the width of the whole wake.

In Fig. 5, averaged vector fields and axial velocity contours in the wake of the models obtained by PIV are depicted for the four tested conditions. In the non-vented configuration, both for the clean and the strip configurations (Fig. 5a, c), the presence of a counter-flow in the wake of the models from the base to approximately $x/D = 1$ is noticed; no large differences are seen between the two configurations, except for a slight reduction of the wake in the strip case. For the vented configurations (Fig. 5b, d) the situation is different; in fact, the venting jet decreases the extent of the recirculation region by penetrating in the wake down to about $x/D = 0.8$ for the clean case, and to about $x/D = 0.9$–1.0 for the strip case (to appreciate this difference, consider the vertical velocity profiles around $x/D = 1$). The difference between strip and clean conditions is caused by the strip that, by forcing the laminar-turbulent transition of the boundary layer, allows a slight downstream displacement of the detachment point thus decreasing the width and increasing the length of the wake (as can be seen from Fig. 1, the models have rounded rear edges to allow such a slight displacement). This is a key point with respect to previous tests performed with sharp edges.

It has to be noticed that in both strip and clean conditions, the venting jet is not able to fully emerge from the wake; thus a minor effectiveness of natural ventilation in comparison with the case of the sphere must be expected. This is confirmed by the fact that for

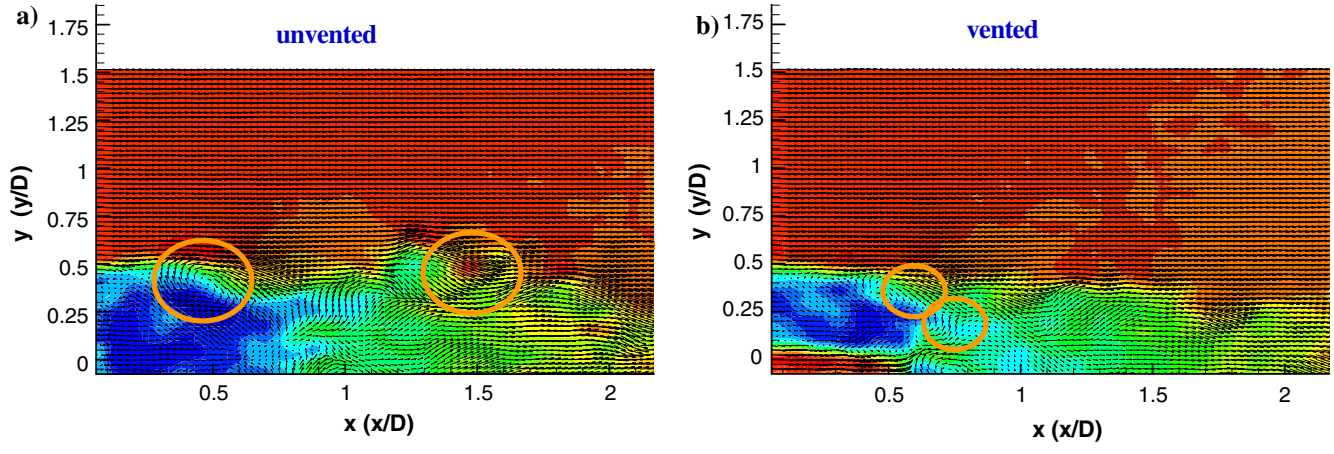

Fig. 4 Instantaneous vector fields and axial velocity contours from PIV: **a** non-vented, strip configuration; **b** vented, strip configuration. $Re = 1.7 \times 10^5$

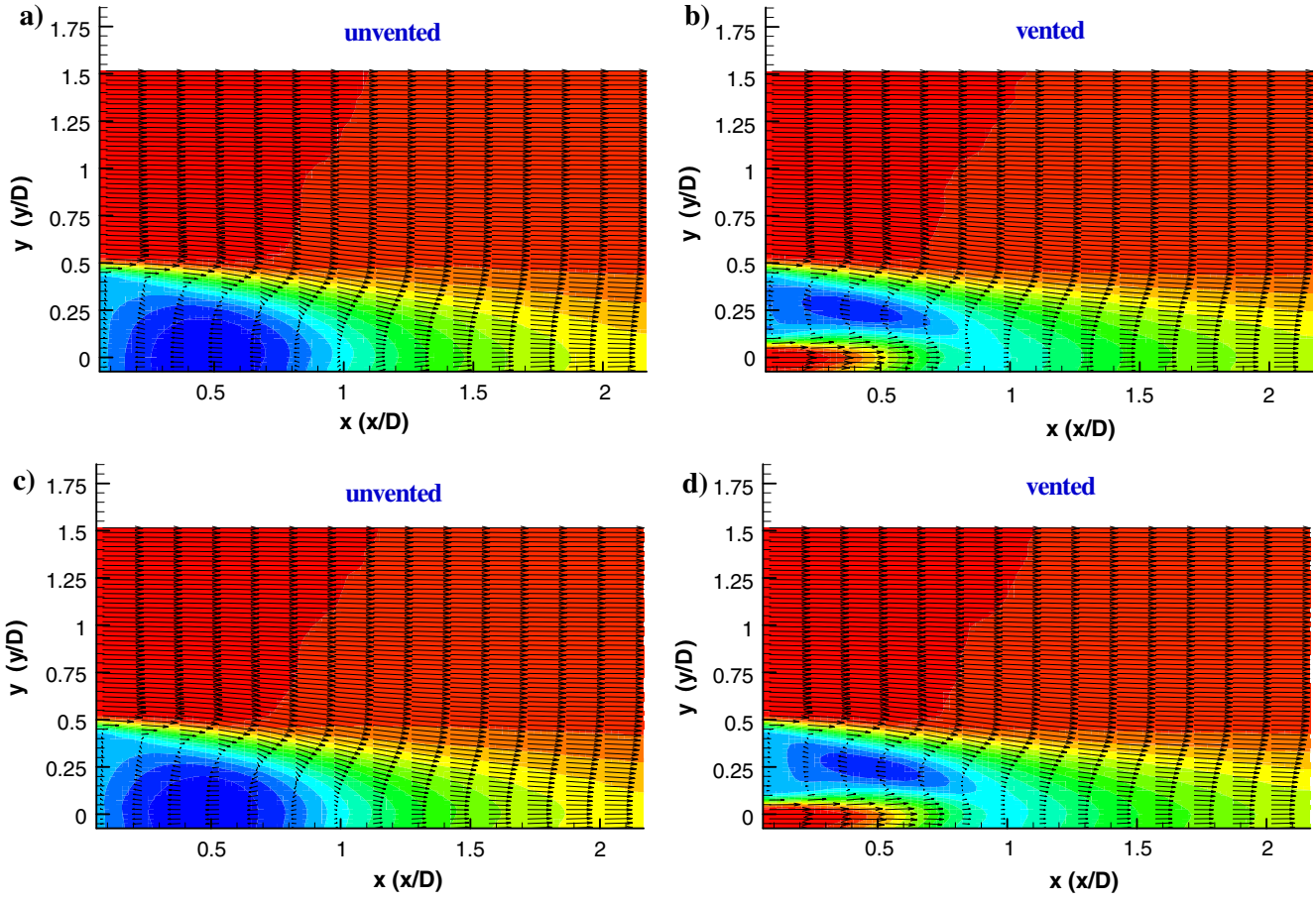

Fig. 5 Averaged vector fields and axial velocity contours from PIV: **a** non-vented, no-strip configuration; **b** vented, no-strip configuration; **c** non-vented, strip configuration; **d** vented, strip configuration. $Re = 1.7 \times 10^5$

$x/D > 1.5$ higher velocities are obtained at the middle of the wake for non-vented models in comparison with the vented. Thus, only some portions of the wake are accelerated when ventilation is active; as a matter of fact, the whole configuration of the wake is changed in comparison with non-vented conditions.

In Fig. 6, the vented configuration with strip and without it are compared (contours of vertical velocity are given to better point out the differences in the wake). The elongation of the wake for the strip in comparison with the no-strip case is here more clearly demonstrated by considering the regions of negative vertical velocities from the shear layer (in blue) and the positive vertical velocity from the venting duct (in red).

The experimental results can be coupled with the full field results obtained with the numerical computations; in Fig. 7, such a field is shown for the non-vented and vented conditions. As can be observed from the figures, the general features of the velocity field are captured by the code; however, different from experimental data, the wake is attenuated in the non-vented case (Fig. 7a), while in the case of venting duct, the jet exit velocity appears small (in comparison with outer velocity) throughout the wake (Fig. 7b). This result is the best that can be obtained using different turbulence and wall models; also due to the results observed in the shear layer, the sensitivity of the numerical code to the used models seems to be high.

Velocity profiles can be derived from previous two-dimensional experimental and numerical data; in Fig. 8, the streamwise component of velocity along transverse and longitudinal directions in the wake of the model are shown. From the transverse profiles immediately downstream of the vented models at $x/D = 0.25$ (Fig. 8a), the overlapping between the different techniques is poor. For HWA, this is due to the unresolved velocity direction in the wake (no negative velocities), while for the Pitot tube this is due to the poor spatial resolution of the method (which smoothes the differences in the profile). It is well known that these techniques are not useful to measure a velocity deficit in the wake of a bluff body where low or reversing velocities can occur; it is also important to consider that the data from the different methods are acquired in rather different conditions (Reynolds number equal to about 3.4×10^5 for the Pitot and HWA measurements and equal to 1.7×10^5 for PIV). This will be particularly relevant when considering rms profiles in the following.

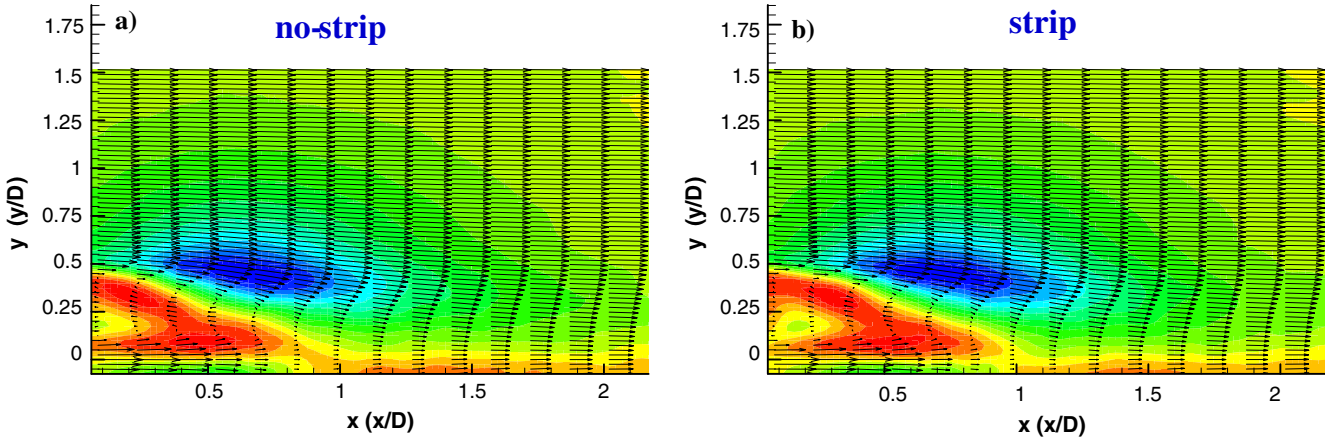

Fig. 6 Averaged vector fields and vertical velocity contours from PIV: **a** vented, no-strip configuration; **b** vented, strip configuration. $Re = 1.7 \times 10^5$

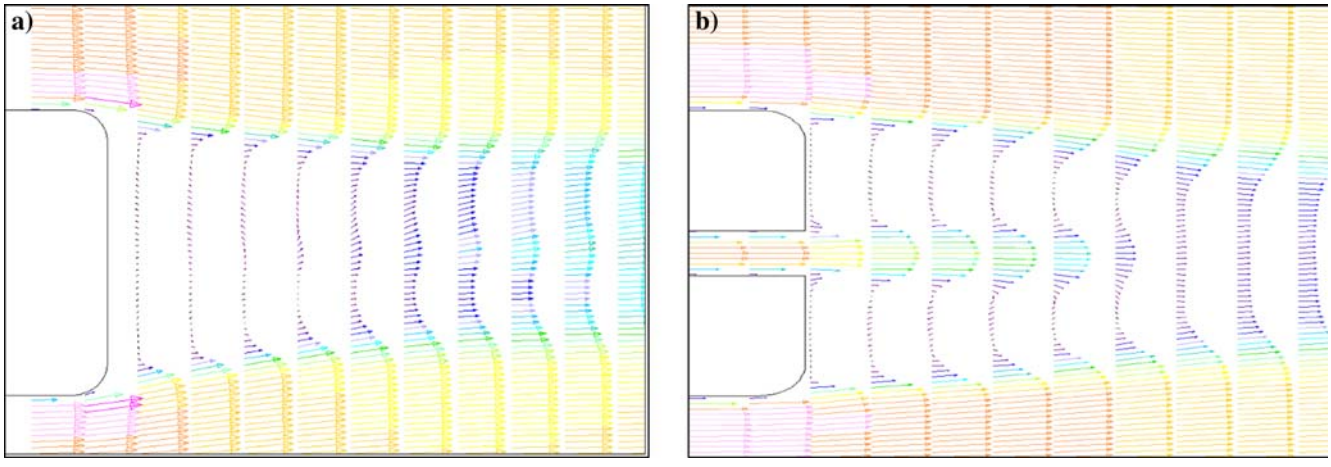

Fig. 7 Vector fields and velocity magnitude (*vector colours*) in the wake of clean (no-strip) models from numerical computations: **a** non-vented and **b** vented conditions. $Re = 2.38 \times 10^5$

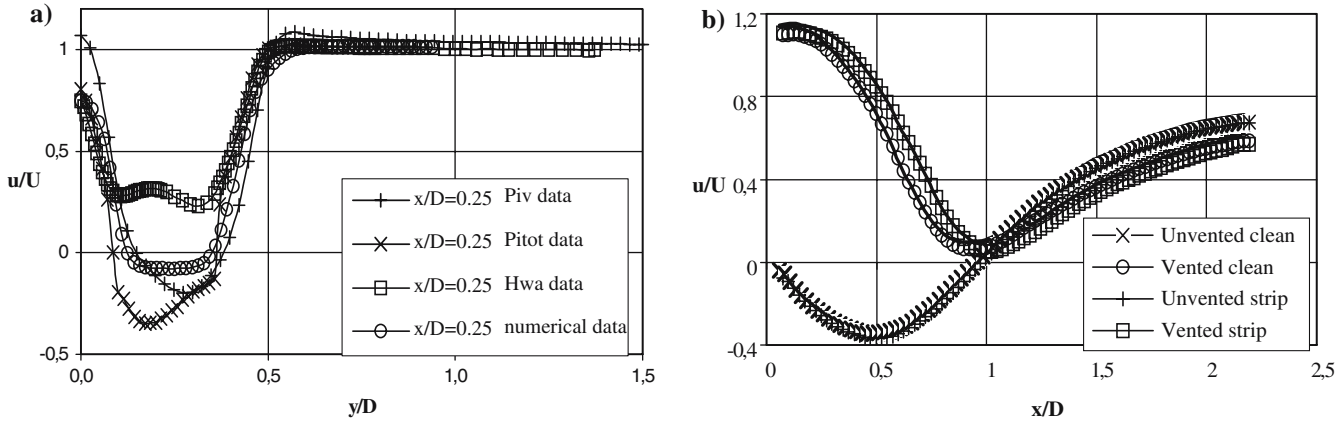

Fig. 8 Streamwise velocity profiles: **a** transverse profile at $x/D = 0.25$ obtained with different techniques for the clean vented model; **b** longitudinal profiles at $y/D = 0$ (*centreline*) obtained from PIV measurements for the different models

It is interesting to compare PIV and numerical results (in this case the difference in Reynolds numbers is much lower than before); from the last, there is a clear underestimation of the absolute values of the negative velocities in the separation region (about one half). Moreover, the profiles for $y/D > 0.5$ (external flow) are

also different; the PIV data show a slight increase in velocity in the shear layer which is not displayed by numerical results. The former result seems to be reasonable due to the increased velocity (in comparison with the free stream) around the bluff body model; the discrepancy with the numerical result is probably due to poor resolution of the numerical grid to describe the external boundary layer in detail.

For the longitudinal profiles (Fig. 8b), it can be observed that the results for non-vented profiles are independent of the presence or not of the strip (as noticed also in Fig. 5). On the other hand, the strip vented profiles clearly show an increase in velocity in the near wake ($x/D < 1$) in comparison with the clean vented one (i.e. an increased length of the wake as also derived from Fig. 5). Moreover, for all vented conditions the wake appears to be more extended along the longitudinal than in non-vented (wake recover is obtained at larger values of x/D).

To compare velocity data with direct force measurements, the drag, Dr, has been computed from measured transverse mean velocity profiles as those presented in Fig. 8a (on cross-sections S (y, φ), φ being the azimuth angle) using the Maskell's formula, modified by Cummings et al. (1996):

$$\mathrm{Dr} = \rho \int_S u(U_\infty - u)\mathrm{d}S + \frac{1}{2}\rho \int_S \left(u^2 - U_\infty^2 + v^2 + w^2\right)\mathrm{d}S \tag{1}$$

where u, v, w are the velocity components evaluated on the given cross-section S in the wake (the w component is unknown for 2 D measurements) and ρ is the fluid density. The drag coefficients have been computed using vertical profiles (along y), assuming axial-symmetry on average (i.e. all mean velocity components are independent on the azimuth φ, the spanwise velocity $w \equiv 0$ on each y profile and the cross section is given by $\mathrm{d}S = \mathrm{d}y\ y\ \mathrm{d}\varphi$). These coefficients have been derived at different axial distances ($x/D = 1, 1.5, 2$); this has been done because the distance at which it is correct to perform the evaluation given by (1) is not always specified in the literature (Oertel 1990). In Table 1, the data are presented for all the models.

Considering the approximate level of the previous relation (1), the data, for the non-vented configuration, can be considered in good agreement with those from the balance. On the other hand, for the vented configurations the differences are much stronger. However, even in this case, a reduction of 5% between vented and non-vented clean models can be derived from measured profiles. It is interesting to note that the data resulting from the velocity profiles decreases as the distance from the model increases; this is obvious due to the recovery of the velocity downstream of the body. In practice, the profiles in the range $x/D = 1$ to $x/D = 1.5$ seem to be better suited for drag measurements for non-vented conditions, while for vented conditions the profiles between $x/D = 1.5$ and $x/D = 2$ more closely resemble the data from direct balance measurements. This is reasonable when considering that the wake for vented conditions is more extended than for non-vented (as confirmed by Fig. 8b). Thus, this confirms findings from other authors, i.e. that drag measurements from velocity profiles in the wake must be derived at locations which depend on the model geometry.

The observed differences depend on the pressure field, not evaluated in the present experiments; pressure plays an important role in the evaluation of the drag from velocity profiles (pressure fields derived from numerical simulations indicate that pressure recovery is far to be obtained at $x/D = 2$). For this reason, pressure measurements are required in future experiments.

A question arises if the observed overall drag reduction in vented conditions, derives from reduction in form drag or in skin friction (or both). Indeed, for the present bluff body models, as pointed out in Sect. 1, the major contribution should be expected from the former. However, it is still interesting to consider the effects of the venting jet on the boundary layer behaviour. To do this, the momentum thickness (θ) has been evaluated from the streamwise velocity profiles in the shear layer ($y/D = 0.5$), from the rear part of the body ($x/D = 0$) to the near wake ($x/D = 0.5$). In Fig. 9, this thickness is reported for the different conditions; from this figure, it is clear that at the separation point ($x/D = 0$) the momentum thickness (non dimensional by the model diameter) is lower for strip in comparison with no-strip conditions

$\theta/D \approx 0.0146$ strip vented
$\theta/D \approx 0.0149$ strip non-vented
$\theta/D \approx 0.0165$ vented clean
$\theta/D \approx 0.0152$ non-vented clean

This means that the shear stress at the wall (and the friction drag) should be higher for strip conditions due to laminar-turbulent boundary layer transition. In particular, the lowest value is attained for the strip vented condition, i.e. the one which exhibits the largest total drag reduction.

Concerning the rate of increase of momentum thickness, it is lower for the vented conditions in comparison with the non-vented. However, while for the strip vented case the rate is constantly lower than the strip non-vented case, for the clean vented case the rate is initially as high

Table 1 Comparison between drag coefficients obtained from PIV velocity profiles for the different models. Direct balance measurements are reported for comparisons

Distances	Non-vented clean	Vented clean	Non-vented strip	Vented strip
1D	0.384	0.332	0.364	0.356
1.5D	0.281	0.275	0.254	0.265
2D	0.190	0.211	0.178	0.200
Balance measurements	0.33	0.27	0.37	0.23

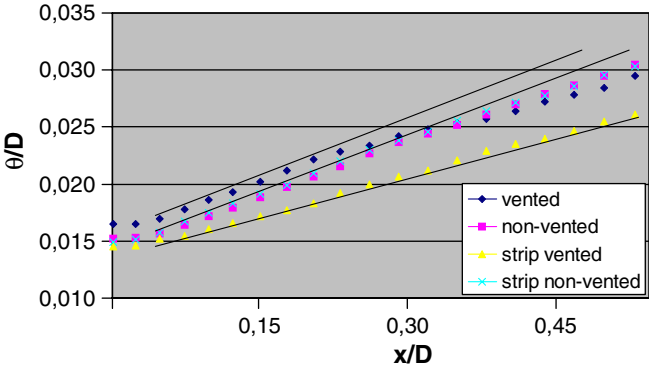

Fig. 9 Momentum thickness behaviour along the streamwise direction obtained from PIV velocity measurements for the different models

as non-vented condition and only from $x/D \approx 0.25$ it becomes lower, probably where effects of the venting jet are sensed. This means that when ventilation is active there is not a separation as large as without ventilation (in agreement with the findings of smaller vortical structures for the vented case). Thus, there is a net decrease in form drag and a slight increase in friction drag for the vented conditions. Of course, for a bluff body the increase in friction drag is much less relevant than the decrease in form drag, so that the net effect is a reduction in total drag.

To better understand the fluid dynamic fields surrounding the models, PIV measurements in front of the bodies have also been performed (Fig. 10). Differences are observed only just in front of the models, at the duct inlet ($x/D = 0$); far upstream the differences in the fluid dynamic field are negligible; as already reported, the momentum differences between the two cases leads to a difference not higher than 2% (difference in cross-sections). These results agree almost perfectly with numerical simulations in front of the bodies as shown in Fig. 11.

Therefore, the measured differences between vented and non-vented models indicate that the drag reduction mechanism in the vented models is only partially due to modifications in front of the body, whereas the main effect is in the bluff body wakes.

3.3 Turbulence and Reynolds stress measurements

It is important to have information about the modification of the turbulent kinetic energy in the wake; in Fig. 12, the streamwise rms velocity profiles (normalised with the free-stream velocity) are given for measurements with HWA and PIV. In the near wake ($x/D = 0.25$), the strong additional peak for the vented case (at $y/D = 0.1$, Fig. 12c) reveals an increase in turbulence of the near wake in comparison with the non-vented case (Fig. 12a). The shear layer peak (at $y/D = 0.5$) is slightly reduced in the vented case, thus confirming an overall redistribution of the kinetic energy. There are quite strong differences between the results obtained with HWA and PIV; the latter underestimate the level of fluctuations of about 20%. This is due to the already considered limitations in HWA techniques in measuring wake flows and to differences in Reynolds numbers between PIV and HWA tests (about a factor 2).

For the profile at $x/D = 2$ (Fig. 12b, d), the turbulence levels are reduced when the venting duct is active; in the non-vented case, the maximum (at $y/D = 0.35$) is about 0.16 (for HWA) and 0.14 (PIV), while for the vented case it is about 0.15 (HWA) and 0.13 (PIV) (and also moved to $y/D = 0.3$, i.e. slightly closer to the centreline). This reduction is observed also at the centreline and in the outer layer; the overall picture displays a reduction in the wake turbulence levels and amplitude thus confirming the observed reduction of turbulence in the wake for the case of the sphere. However, for a bluff body, the amount of reduction is lower than for the sphere even if still interesting for practical applications.

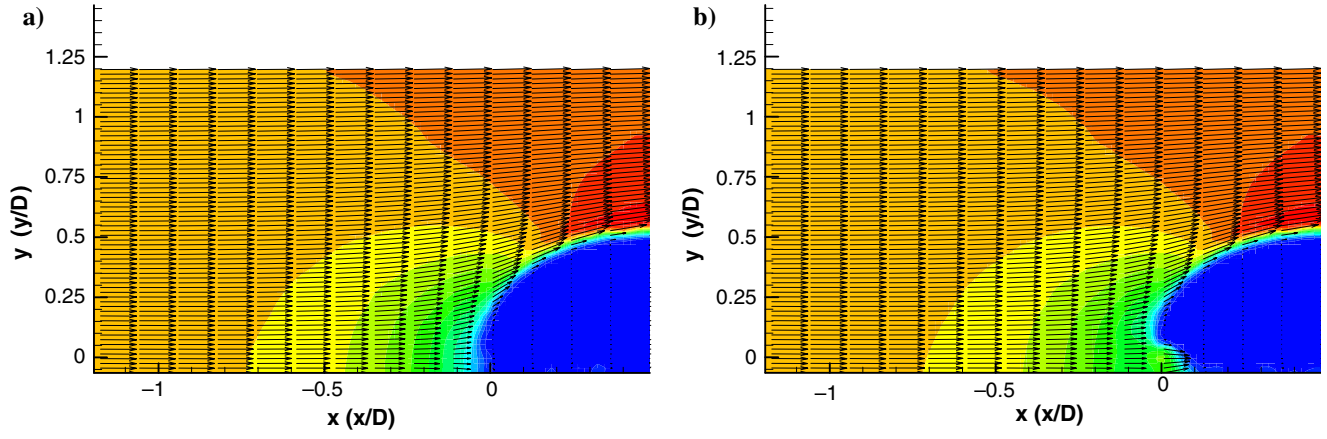

Fig. 10 Averaged vector fields and axial velocity contours in front of clean (no-strip) models from PIV: **a** non-vented and **b** vented conditions. $Re = 1.7 \times 10^5$

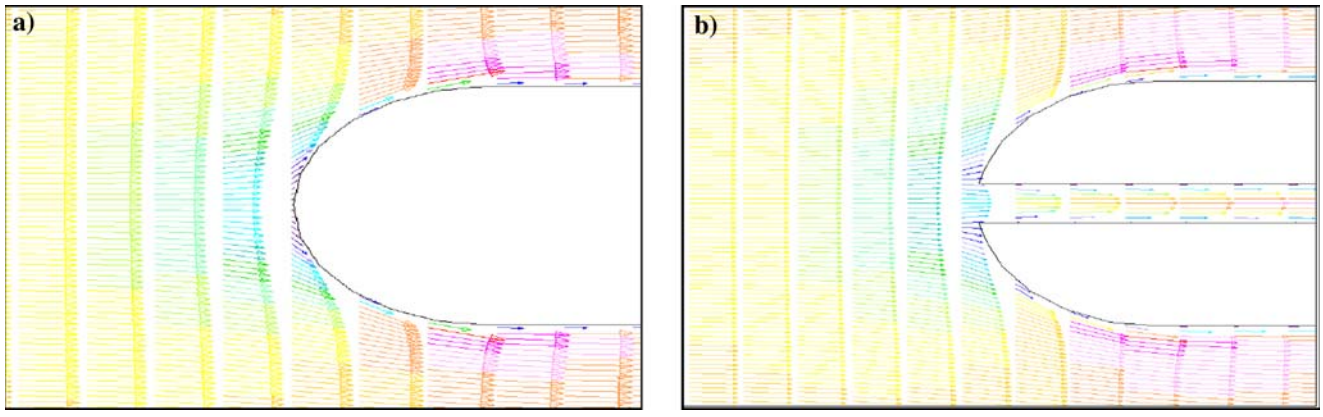

Fig. 11 Vector fields and velocity magnitude (*vector colours*) in front of clean (no-strip) models from numerical computations: **a** non-vented and **b** vented conditions. $Re = 2.38 \times 10^5$

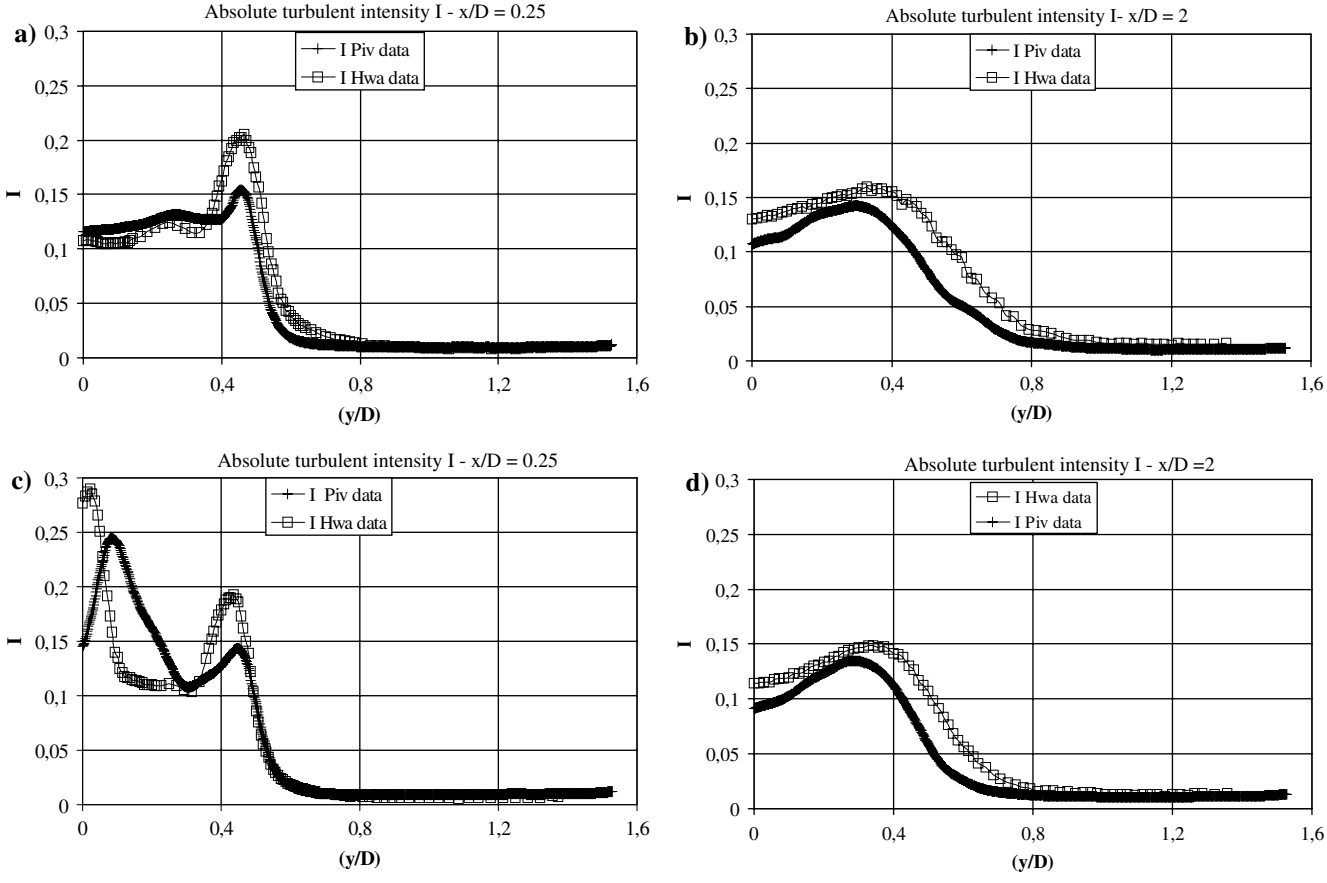

Fig. 12 Turbulence intensity profiles measured by PIV and HWA; non-vented models at **a** $x/D = 0.25$ and **b** $x/D = 2$; vented models at **c** $x/D = 0.25$ and **d** $x/D = 2$

In Fig. 13, the Reynolds stress obtained from PIV for the different configurations are shown. Two main points can be noted. First, the vented configurations present smoothed local minima with respect to the non-vented configurations (compare Fig. 13b, d with Fig. 13a, c). Secondly, a complete redistribution of the stresses over the whole wake (and a general reduction in the wake amplitude) takes place.

In particular, a slight downstream displacement can be noted for the local maxima and minima of the stress in vented strip configuration with respect to the vented no-strip one (compare Fig. 13d with b). These findings confirm the reduction in turbulence fluctuations and in the amplitude of the wake already observed from other measurements.

3.4 Spectra

From HWA data it is also possible to evaluate power spectral densities of the velocity at different points of the wake (the data rate of the HWA data is sufficiently high to detect vortical structures from the shear layer and from the venting duct). In Fig. 14, three spectra obtained from measurements in the shear layer ($x/D = 0.5$, $y/D = 0.45$) ($x/D = 1$, $y/D = 0.45$) and at the centreline ($x/D = 0.5$, $y/D = 0$) are given for the strip configuration in vented and non-vented conditions (in the horizontal axis the Strouhal number, $St = fD/U$ rather than the frequency f alone is given). In the shear layer close to the model (Fig. 14a), for the non-vented case, a distinct peak at $St \approx 0.22$ is obtained; this is just the value expected for wake vortices released behind bluff bodies, i.e. for vortex shedding conditions. The flow visualisations in Fig. 2b also confirm the presence of vortex shedding patterns at the considered HWA measurement position ($x/D = 0.5$, $y/D = 0.45$). Moreover, as already observed, the instantaneous vector plots from PIV measurements (Fig. 4) allow to detect (although only qualitatively) large scale vortices in the near wake (indicated by the orange circles in Fig. 4a). On the other hand, in the vented case, the peak disappears indicating that large scale shedding vortices are suppressed; this is also confirmed by visualisations (Fig. 2c) and PIV instantaneous measurements (Fig. 4b). From the analysis of Fig. 14a, in the vented case, the energy related to large scale vortices seems to be redistributed towards high frequency vortical structures. To quantify this redistribution, spectral slopes are computed from the data; differences among vented and non-vented conditions are revealed. For the non-vented case (which has a single shear-layer), a $-5/3$ slope definitely appears, thus indicating some approach to local equilibrium. For the vented case (with interaction of a outer and inner shear layer due to the presence of the vented jet), no such equilibrium is evident, as shown by the smaller slope (about -0.7), indicating energy production at different wave numbers.

For the non-vented data obtained at the second location downstream in the shear layer (Fig. 14b), the primary peak observed in the non-vented case is attenuated, while the second peak at $St \approx 0.16$ (probably due to secondary vortical structures developing in the shear layer) is emphasised. Also the extension of the region in which the $-5/3$ slope is observed is reduced. Moreover, the whole large scale contribution for the vented data is attenuated. The picture is similar to that derived from the previous location although at this position the spectral redistribution of the kinetic energy takes place

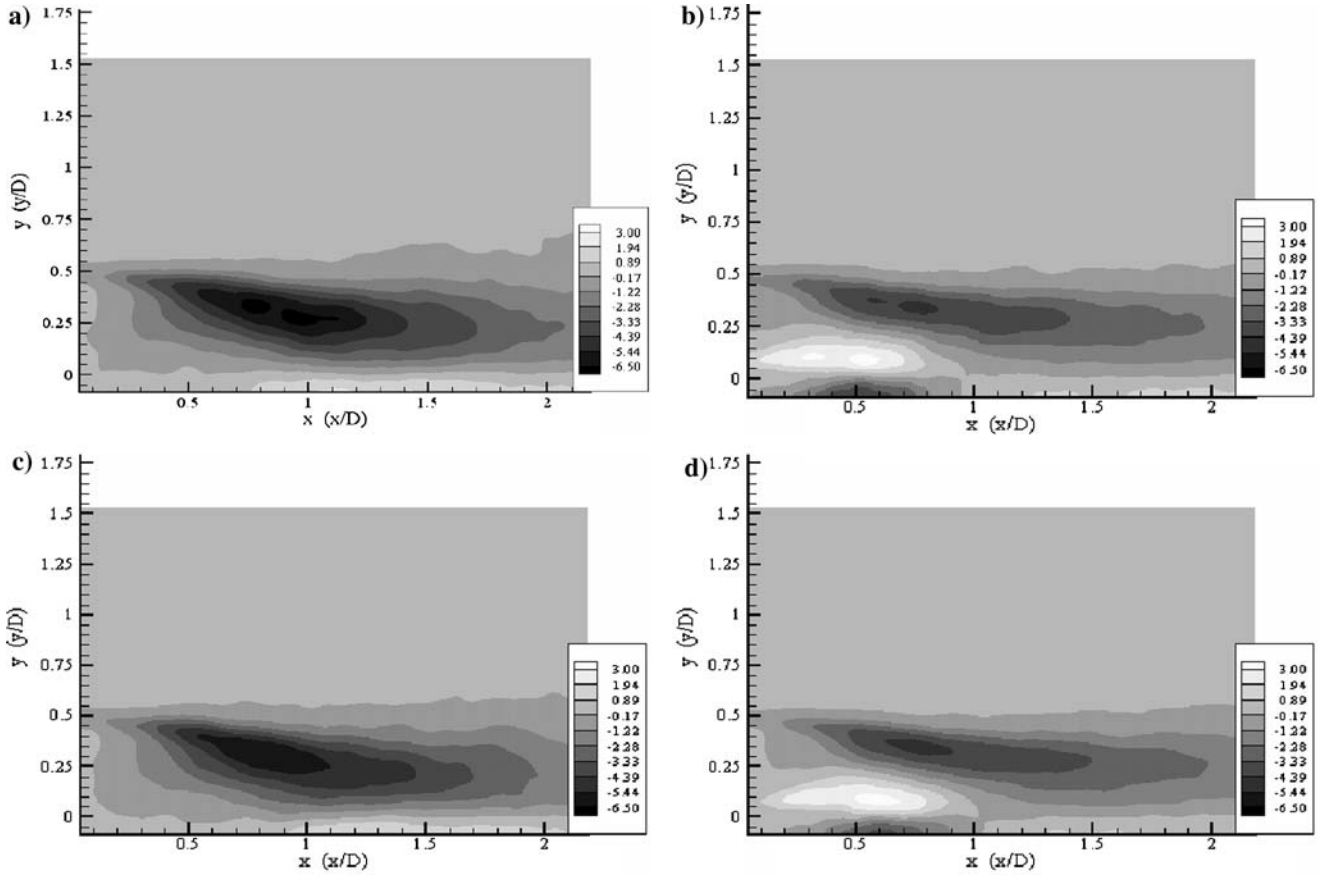

Fig. 13 Contours of Reynolds stress measured by PIV: **a** non-vented, no-strip; **b** vented, no-strip; **c** non-vented, strip; and **d** vented, strip

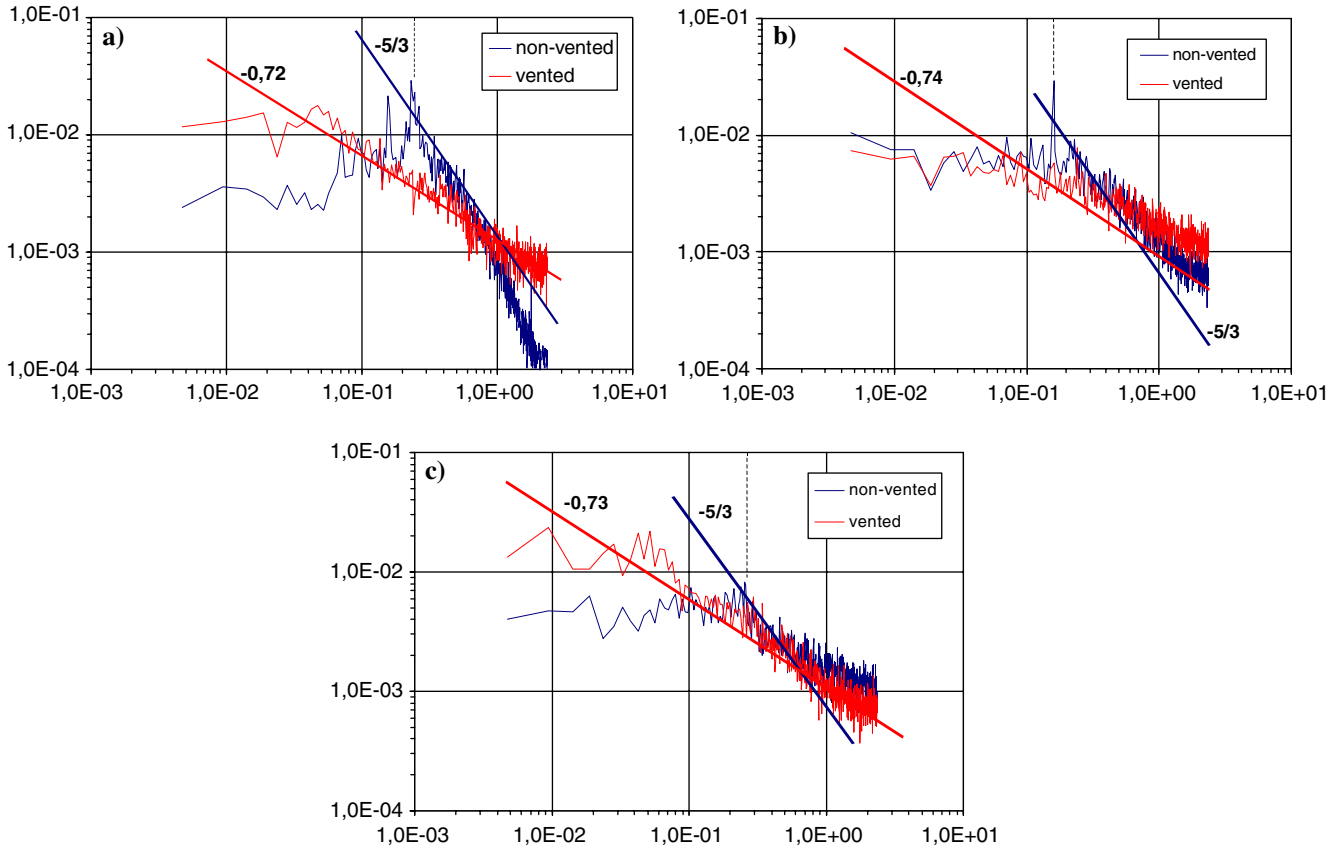

Fig. 14 Power spectral densities (and derived slopes) as a function of Strouhal number obtained from HWA in strip conditions at **a** $x/D = 0.5$ and $y/D = 0.45$, **b** $x/D = 1$ and $y/D = 0.45$, **c** $x/D = 0.5$ and $y/D = 0$, non-vented (*blue*) and vented (*red*) conditions. $Re = 3.3 \times 10^5$

for both vented and non-vented (on a lower extent) conditions.

In the spectra obtained at the centreline (Fig. 14c), large scale contributions almost disappear for the non-vented case while are still present for the vented case; this is due to vortical structures appearing in the second shear layer generated at the borders of the vented jet. As previously, this aspect is qualitatively confirmed by the analysis of flow visualisations (Fig. 2) and PIV instantaneous measurements (Fig. 4b). Thus, the results from spectral analysis point out a strict link between the behaviour in space (which differs from the external to the internal shear layer) and the redistribution of kinetic energy in frequency domain for the vented in comparison to the non-vented case; this confirms the findings derived from direct balance and PIV-HWA measurements.

4 Conclusions

In this work, the passive (or natural) ventilation technique, applied to a bluff body has been studied by means of different experimental and numerical techniques. For the models investigated (without and with turbulence inducing strip on the surface) a drag reduction from direct balance measurements has been valuated both for the clean (7–8%) and the strip configuration (20%). Therefore, the technique seems to work better on rough (i.e. strip) rather than smooth (clean) surfaces; this is quite important for practical applications where aerodynamic surfaces are not really smooth and there is always some degree of roughness. The amount of drag reduction is also dependent on the Reynolds number involved; the reduction is particularly effective for Reynolds numbers around 5×10^5. This is an important point to be considered for applications to relatively low speed vehicles.

The use of round rear edge models allows a displacement of the separation point to take place. This is also another key point for applications of the technique and it can be readily achieved due to the small curvature radius involved.

Experimental and numerical results on the velocity fields in front and in the wake of the models clarified the phenomena involved; a reduction of the wake width, an increase of the wake length and a redistribution of the kinetic energy and turbulent (Reynolds) stress have been measured in the vented conditions in comparison to the non-vented case. This phenomena are mainly due to the interaction between the external shear layer and the jet flowing out of the venting duct; the net effect is a reduction in size and energy of the external vortices by

coupling with the counter rotating vortical structures from the jet. The analysis of spectra in the wake of the models confirms that in the vented case kinetic energy is subtracted from the low frequency vortical structures towards the high frequency ones except for the region close to the venting jet (where another shear layer develops). Negligible differences have been observed in front of the vented or non-vented models, so that the gain in momentum due to the venting jet can account only for a small portion of the observed drag differences (a crude evaluation gives about 2% gain for the vented case). On the other hand, the external boundary layer and the shear layers in the wake seem to be dependent on the presence of the venting jet. A slight increase in friction drag should be expected in venting conditions; however, this increase is very small in comparison to the strong decrease in form drag (as expected for a bluff body).

There is a substantial agreement between the experimental and numerical results (thus confirming the applicability of commercial advanced codes to this sort of problems), even if some underestimation of the wake defect and of the shear layer thickness is obtained from the numerical results.

The evaluation of the force made from the velocity profiles (considering that the applicability of this evaluation is still debated especially from the point of view on the downstream distance to be considered) confirms the observed reduction, although by a smaller magnitude (about 5%); in any case, the amount appears interesting for practical applications. Pressure measurements over the whole model surface are planned for the future for better quantifying the drag reduction mechanism.

References

Achenbach E (1972) Experiments on the flow past spheres at very high Reynolds numbers. J Fluid Mech 54:565–575

Achenbach E (1974) Vortex shedding from spheres. J Fluid Mech 62:209–221

Cummings RM, Giles MB, Shrinivas GN (1996) Analysis of elements of drag in three-dimensional viscous and inviscid flow, AIAA, paper no 962482

Gad El Hak M (2000) Flow control: passive, active, and reactive flow management. Cambridge University Press, Cambridge

Monkewitz PA (1992) Wake control, in bluff body wakes; dynamic and instabilities. In: Iutam symposium, Gottingen

Oertel H Jr (1990) Wakes behind blunt bodies. Annu Rev Fluid Mech 22:539–562

Rae WH, Pope A (1984) Low-speed wind tunnel testing. Wiley Interscience, New York

Roshko A (1961) Experiments on flow past a circular cylinder at very high Reynolds number. J Fluid Mech 10:345–356

Suryanarayana GK, Meier GEA (1985) Effects of ventilation on the flow field around a sphere. Exp Fluids 19:78–88

Suryanarayana GK, Pauer H, Meier GEA (1993) Bluff body drag reduction by passive ventilation. Exp Fluids 16:73–81

Suryanarayana GK, Prabhu A (2000), Effect of natural ventilation on the boundary layer separation and near-wake vortex shedding characteristics of a sphere, Exp Fluids 29:582–591